Modeling Laterally-Contacted nipi-Diode Radioisotope Batteries

Cory D. Cress, *Student Member, IEEE*, Brian J. Landi, and Ryne P. Raffaelle

***Abstract*—A framework for modeling the power generation of laterally-contacted *n*-type/intrinsic/*p*-type/intrinsic (*nipi*) diodes coupled with an alpha-particle radioisotope source is developed. The framework consists of two main parts, the alpha-particle energy deposition profile (*ADEP*) and a lumped parameter equivalent circuit model describing the *nipi* device operation. Experimental measurements are used to verify the *ADEP* modeling approach which determines the spatially varying energy deposited within the device. Using these results, *nipi*-diode radioisotope batteries are simulated and the effect of the number of junctions, the thickness of the junction, and the alpha-particle flux on output voltage and power are investigated. The modeling results indicate that a 1 cm^2 bi-layer device (consisting of one source and two adjacent *nipi*-diodes) with a source activity of 300 mCi can reach a power output of 2 mW, excluding radiation damage effects.**

***Index Terms*—Displacement damage dose profile, InGaP photovoltaic, micropower devices, NIEL, radioisotope batteries, SRIM.**

I. Introduction

THE power and energy densities of radioisotopes have motivated the development of various direct conversion radioisotope batteries schemes aimed at capitalizing on the large theoretical potential of such devices. As illustrated in Fig. 1, radioisotope-based power generation devices offer between 4 and 6 orders of magnitude more power per cubic centimeter than do idealized chemical battery systems, hydrogen conversion, and vibrational or photovoltaic energy harvesting systems (EHS) of comparable lifetimes [1]. The number of available radioactive isotopes enables the choice of fuel to be made application specific, allowing trade-offs between the power, the lifetime, and the cost of the radioisotope power supply to be made (see Fig. 1). From this figure, it is evident that alpha-emitting radioisotopes have an advantage in power density of 1–2 orders of magnitude over beta-emitting isotopes with similar half lives; however, the advantage in power output is often negated by the greater rate of degradation caused by alpha-particles [2]. Advances in photovoltaic production has resulted in direct conversion radioisotope batteries with increased power conversion efficiencies under both alpha and beta particles [3], [4], [6], yet commercially viable direct conversion devices that maintain a long lifetime and are capable of delivering a high power output are yet to be demonstrated.

Manuscript received November 2, 2007; revised January 7, 2008. This work was supported in part by the U.S. Department of Defense. The work of C. D. Cress was supported by NASA under GSRP Fellowship Award NNX07AR57H.

The authors are with the Rochester Institute of Technology, Rochester, NY 14623 USA (e-mail: cdc2798@rit.edu; bjlsps@rit.edu; rprsps@rit.edu).

Color versions of one or more of the figures in this paper are available online at http://ieeexplore.ieee.org.

Digital Object Identifier 10.1109/TNS.2008.920263

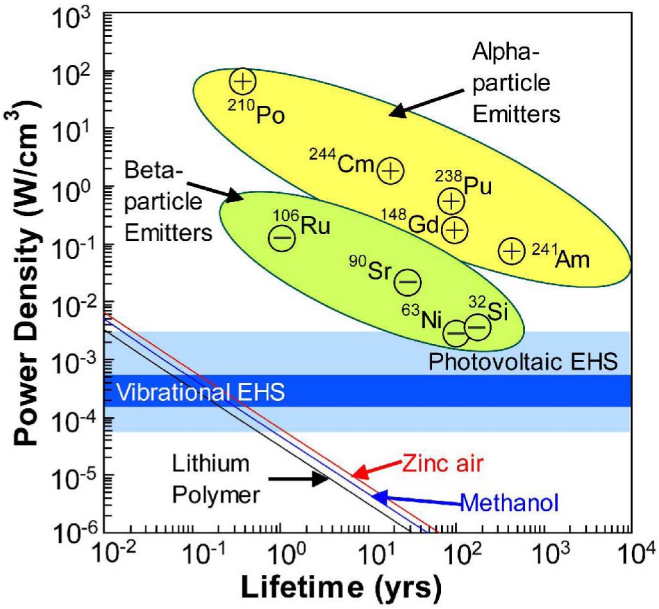

Fig. 1. Theoretical power density versus operating lifetime for various forms of electrochemical cells, energy harvesting and scavenging devices (EHS), and devices based on alpha- and beta-particle emitting radioisotopes. Radioisotope values correspond to the power density at a time equal to 1 half-life assuming a 20% conversion efficiency with half of the volume comprised by the converter. The electrochemical devices were assumed to have a constant voltage throughout their lifetime and half of the volume is comprised by packaging. The vibrational and photovoltaic EHS device power densities were obtained from [1].

A number of strategies may be employed to improve the performance of direct conversion radioisotope batteries. Improvements in radioisotope battery lifetimes may be accomplished through the use of radiation tolerant materials including SiC, InP, and InGaP [3], [5], [6]. Such materials typically display a greater radiation tolerance due to their high threshold for lattice dislocations [7], [8]. In the case of InP, enhanced radiation tolerance is observed as a result of the room temperature annealing effect [5]. An additional benefit of wide bandgap materials (i.e., SiC and InGaP) is a reduced intrinsic carrier concentration which leads to a lower dark current. This enables greater efficiencies to be achieved under lower fluxes and a wider operating temperature range [4]. Utilizing a p-type/intrinsic/n-type (*pin*) or *nip* device configuration has been shown to further reduce dark current and the susceptibility of minority carriers to recombination at lattice defects via drift field carrier extraction [3].

For radioisotope batteries which employ an alpha-particle source novel device structures have been proposed to improve their longevity and efficiency [2]. A design in which the alpha particle comes to rest outside of the junction is a potential means to reduce the rate of degradation since most of the damage is imparted by the particle at the end of its range.

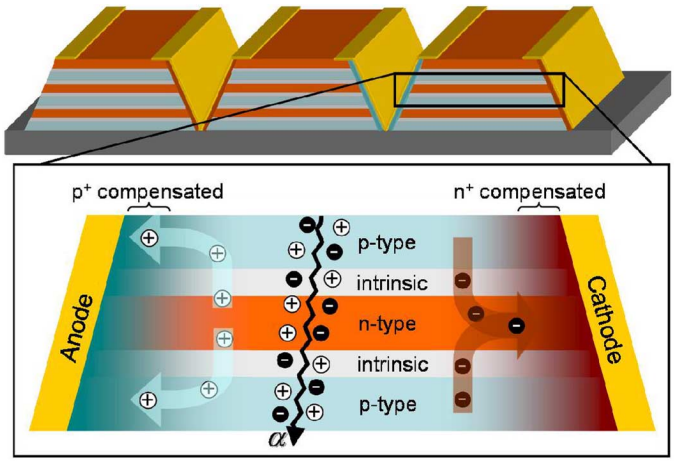

Fig. 2. Schematic depicting the multilayered structure of the *nipi* device. The arrows indicate the direction of electron (designated with "−") and hole "+" transport and subsequent collection to the external contacts of the device.

Three dimensional junctions are device architectures that have been proposed as a means to increase the nuclear absorption cross section so as to enhance the conversion efficiency of direct conversions devices. Such devices may be fabricated by diffusion into surface-machined or porous semiconducting materials (e.g., porous silicon [9]) or by epitaxial growth of a vertically stacked homojunctions [10].

The vertically stacked multiple-homojunction device consisting of repeating p-type/intrinsic/n-type/intrinsic layers (*nipi*) (see Fig. 2) may be able to capitalize on nearly all of the aforementioned techniques for increased radiation tolerance and conversion efficiency. The multiple junctions greatly increase the absorption cross section allowing for full absorption of energy within the active region of the device. An enhancement in radiation tolerance, above that obtained by the drift field in a single *pin* structure, may be achieved by the two dimensional transport of carriers out the device. Such operation is obtained by separating carriers in the direction perpendicular to the junction while transport out of the device takes place through lateral diffusion of excess majority carriers to selectively doped regions (see Fig. 2). Selectively doped regions may be fabricated by V-groove etching followed by epitaxy re-growth, ion implantation, or "smart metallization." Smart metallization refers to contacts made ohmic or rectifying to the various n-type/p-type layers through deposition of metal alloys with appropriate work functions to compensate the semiconductor near the metal contact [11], [12]. A macroscopic device is created by extending the alternating the n-type and p-type grid fingers to bus bars on opposite ends of the device.

The focus of this paper is the development an empirically based model for predicting the steady state current versus voltage output of a *nipi* device under an isotropic alpha-particle source. This model is used to determine how the number of junctions, the junction thickness, and level of flux affect the steady state power output of the device. The *nipi* device is simulated using a lumped parameter equivalent circuit of identical diodes connected in parallel. Experimentally measured single diode parameters are used as the parameter inputs. Using a revised form of the alpha-particle energy deposition profile (*ADEP*) formulation reported in [3], it is shown that the *ADEP* can be related to the short circuit current of a single diode, and subsequently used as the alpha-generated current for each of the diodes within the *nipi* structure. To illustrate the approach, the diode parameters used in the lumped parameter equivalent circuit model are extracted from current versus voltage measurements of a wide bandgap semiconductor diode comprised of $In_{.48}Ga_{.52}P$; however, the framework presented here can easily be extended to diodes grown from any material system.

II. Experimental Details

The $(1.0 \times 1.0$ cm $^2)$ InGaP devices used to generate the model inputs have p^+n shallow homojunctions consisting of a 0.1 μm 1e18 Zn-doped $In_{0.48}.Ga_{0.52}P$ p-type emitter and a 1.0 μm 1e17 Si-doped $In_{0.48}.Ga_{0.52}P$ n-type base sandwiched between a 0.02 μm AlAs p^+ window and a 0.05 μm AlInP n^+ back surface field layer epitaxially grown on n -type GaAs wafers. The top side grid contained a tapered bus bar down the middle of the device with 25 grid fingers (spaced $\sim$400 μm apart) and was patterned using a Karl Suss contact aligner. The top-side metal contact (20 nm Au, 20 nm Zn, and 1 500 nm Au) and back-side metal contact (25 nm Ge, and 1500 nm Au) were deposited by thermal evaporation and annealed at 420°C and 380°C, respectively. The current–voltage $(I$–$V)$ response of the diodes under various levels of excitation power were measured using a LabVIEW controlled Keithley 237 SMU in the remote sense mode. The I–V measurements were made on the diode under various levels illumination (12-watt fluorescent ring-light), controlled by varying the diode-to-bulb distance and angle. Two to three measurements were obtained per decade of short-circuit current, I_{sc}, ranging from 10^{-9} to 10^{-2} mA/cm^2. In an analogous manner, the I–V response of the diode under various levels of α -particle flux was measured at incremental diode-to-source (^{210}Po 5.35 MeV α-particles) distances. For these measurements, the distance was varied from 3.0 mm to 12.5 mm in 0.5 mm increments and controlled using a micropositioning stage with an accuracy of 50 μm. The source had an areal activity of 0.14 mCi/cm^2 and a total circular area of 2.5 cm ^{2}.

III. Modeling Framework

A. Alpha-particle Deposition of Energy Profile (ADEP)

The spatial energy flux, *ADEP*, deposited within a differential volume, *dv*, in the cell is modeled as

$$\mathbf{ADEP}(\varphi, v) = \frac{\mathbf{dv}\,\varphi}{2\pi \mathbf{A_s}} \int_0^{\mathbf{R_s}} \int_0^{2\pi} \frac{(\mathbf{G_a} + \mathbf{z_c})\mathbf{r_s}}{\|\vec{\mathbf{l}}\|^3} \frac{\mathbf{dE}}{\mathbf{dx}}(\mathbf{l_{c,eff}})\, \mathbf{d\theta_s}\, \mathbf{dr_s} \quad (1)$$

where the integration is taken over then entire surface area of the extended alpha-particle source of area A_s, radius R_s, and activity φ. The air gap between the source and device is G_a, the depth into the cell is z_c, and the vector extending from a point on the source to the differential volume is, $\vec{l} = [r_s \cos\theta_s - r_c \cos\theta_c, r_s \sin\theta_s - r_c \sin\theta_c, G_a + z_c]^T$, where r_s and θ_s define positions on the source and r_c, θ_c, and z_c, define the position

of the differential volume. The function *dE/dx* is the ionization energy loss rate of alpha particles in InGaP, which depends on $l_{c,\mathrm{eff}}$, the effective path length in InGaP

$$\boldsymbol{l_{c,eff}} = \boldsymbol{l_c} + \Re_{\boldsymbol{c}}(\boldsymbol{E}_0) - \Re_{\boldsymbol{c}}(\boldsymbol{E_{air}}(\boldsymbol{l_a})). \tag{2}$$

In (2), E_{air} is the energy of the alpha-particle as a function of the distance traversed in air l_a starting with an initial energy E_0. The function $\Re_c(E)$ is the range of alpha particles in InGaP as a function of energy, and l_c is the physical distance traversed in the diode. To obtain a functional form for $E_{\mathrm{air}}(x)$, the procedure from [13] was adopted. The range versus energy for alpha particles in air and in InGaP were obtained from SRIM 2003; *dE/dx* was also obtained from SRIM 2003, from a simulation with detailed tracking of damage for 20 000 alpha-particle histories starting with an initial energy of 5.35 MeV and normally incident with $In_{0.5}Ga_{0.5}P$ with a density of 4.517 g/cm^3 [14]. In the final form of (1), the relationship, $\cos\phi = (G_a + z_c)/||\vec{\mathbf{l}}||$ has been used, where ϕ is the angle between the normal to the alpha-source source and the position vector $\vec{\mathbf{l}}$. The cosine term is related to the solid angle subtended by the source as viewed from a position within the cell. No projected area correction is required for the area of the cell absorbing the radiation since it has a finite depth and therefore can accept radiation equally from all directions (i.e., a point radiation "acceptor").

The above formalization can also be extended to the non-ionizing energy loss (NIEL) of the particle within the diode. To accomplish this, the flux φ in (1) is replaced with the total fluence Φ and the ionization energy loss rate *dE/dx* is replaced with the NIEL (x) using the procedure found in [13]. A 3 eV binding energy loss was assigned to each vacancy and displacement threshold energies of 6.7 eV, 10 eV, and 8.7 eV, were used for In, Ga, and P, respectively [13]. This calculation yields the displacement damage dose profile (D^3P) in units of MeV/($g\cdot$ cm^3) and provides a spatial representation of the damage generated within the device. (Integration of the displacement damage dose profile over the entire device volume yields the displacement damage dose for the entire cell in the common units of MeV/g.)

B. Equivalent Lumped Parameter Nipi Circuit Model

A lumped parameter equivalent circuit model was employed as a simple means to simulate the I–V response of a *nipi*-based alpha-voltaic battery. The variables investigated here include the number of junctions in the stack, the thickness of the layers, and the alpha-particle flux. However, the effects of doping concentrations, contact separation, etc., may also be incorporated into the model simply by generating an empirical data set resulting from measurements of single junction devices. The purpose of such a model is to provide a theoretical framework for estimating the power output of a *nipi* device, based on empirically measured single junction devices, and to optimize the device structure prior to growth.

The I–V relationship of a *nipi* diode can be modeled by the following three-component lumped parameter equivalent circuit model summed over each diode i in the N—junction device [15]:

$$\begin{aligned}\boldsymbol{I} = \sum_{i=1}^{N} \Bigg\{ & I_{o1_i}\left(1 + 2\boldsymbol{g}A_{\mathbf{i}}\right)\left[e^{V/n_1 V_{\mathrm{th}}} - 1\right] \\ & + \mathbf{I}_{o2_i}\left(1 + 2\boldsymbol{g}A_{\mathbf{i}}\right)\left[\boldsymbol{e}^{V/n_2 V_{\mathrm{th}}} - 1\right] \\ & - \boldsymbol{I_{\alpha_i}} + (1 + 2gA_i)\frac{\boldsymbol{V}}{\boldsymbol{R}_{SH}(\mathbf{I}_{\alpha_i})}\Bigg\},\end{aligned} \tag{3}$$

where I_{o1} and I_{o2}, represent the diffusion and recombination saturation currents with the respective n_1 and n_2 ideality parameters, g is the number of grid fingers, A is the ratio between the junction area formed at the grid fingers to the vertical junction area. Furthermore, V_{th} is the thermal voltage, I_α is the alpha-particle generated current, and $R_{\mathrm{SH}}(I_\alpha)$ is the active-state shunt resistance which depends on I_α. Although shunt resistance is accounted for, no series resistance term is included since the current levels considered are on the order of 10^{-3} A/cm^2 or less and carrier extraction occurs in the highly doped regions lateral to the device. The edge diodes created at the contacts by the selective metallization are included in the model (i.e., through the $2gA_i$ terms) and are modeled to be identical to the main vertical junctions with the current scaled in proportion to the area of the grid finger junctions.

Analogous to a solar cell under illumination, the alpha-generated current I_α is proportional to the total incident energy absorbed within the active region of the device. Since the *ADEP* is spatially dependent within the device stack it is necessary to independently determine the I_α for each cell in the N-cell stack. Taking η_α as the proportionality constant, the total alpha-generated current for cell i, of volume v_i, in a multijunction device of total volume v is

$$\boldsymbol{I_{\alpha_i}}(\boldsymbol{\varphi}) = \boldsymbol{\eta_\alpha} \int_{v_i} \boldsymbol{A}DEP\,(\boldsymbol{\varphi}, \boldsymbol{v})\boldsymbol{d}v_{\boldsymbol{i}}. \tag{4}$$

In this equation, the ADEP term is dependent on the location of each cell volume and is the source of the flux-dependent total current in (3).

Inspection of the measured I–V response of the InGaP test diode under increasing photon and alpha-particle excitation power revealed a decreasing shunt resistance under short circuit conditions. This causes the superposition assumption for a diode under illumination (i.e., the linear addition of the illumination current with the dark current) to be valid only for small variations in excitation power [15]. To account for the intensity dependent low-bias I–V slope, thereby enabling a wider range of alpha-particle fluxes to be simulated, this effect was lumped into the shunt resistance term as follows:

$$\boldsymbol{R_{SH}}(\boldsymbol{I_\alpha}) = \frac{\boldsymbol{R_{SH_0}}}{1 + \boldsymbol{k}\boldsymbol{I_\alpha}}. \tag{5}$$

In this equation, R_{SH0} is the shunt resistance under dark conditions, while k is a free fitting parameter. The physical origin of this excitation dependent resistance may be related to carrier generation in the depletion region and the subsequent depletion width narrowing. Both effects will reduce the barrier to forward

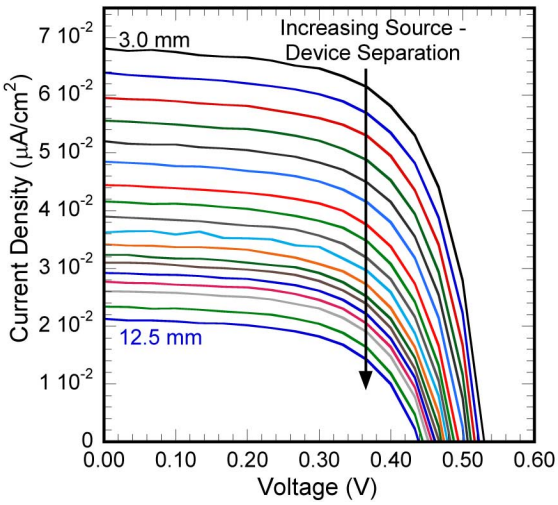

Fig. 3. Current density versus voltage response of an $p + n$ InGaP diode with increasing ^{210}Po alpha-particle source–device separation distances.

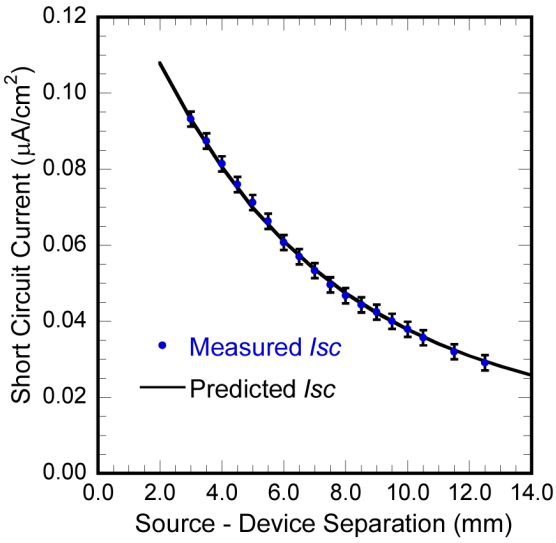

Fig. 4. Measured and predicted [based on (4)] short circuit current density versus alpha-particle source–device separation.

injection and recombination current (or increase the collection efficiency under reverse biased conditions). Curve fitting of the excited-state shunt resistance versus I_{sc} based on the measured I–V curves for increasing photo and alpha-particle excitation rates allows the values of R_{SH0} and k to be determined (see Section IV).

IV. Results and Discussion

A. ADEP Model Verification

Depicted in Fig. 3 are the current versus voltage curves for the measurements taken at increasing alpha particle source–device separations as discussed above. As expected, the peak power output was obtained for the 3.0 mm source–device separation and slowly decreases as the separation increases. Two power conversion efficiency metrics can be defined for a radioisotope battery in this configuration: a) the external efficiency

$$\eta_e \equiv \frac{P_{mp}}{E_\alpha \varphi_s} \tag{11}$$

which is the ratio between the electrical power generated by the device P_{mp} to the total alpha-particle energy emitted from the source per unit time, where E_α is the energy of the emitted particle; and b) the internal efficiency

$$\eta_i \equiv \frac{P_{mp}}{\int_{v_a} ADEP\,(\varphi, v)\, dv_a} \tag{12}$$

which is a ratio between the electrical power generated by the device to the rate of alpha-particle energy deposited within the active region of the device v_a. It is apparent that an accurate *ADEP* model is required to correctly determine the internal efficiency metric. It is important to note that the external efficiency can be doubled if the alpha-particle source is sandwiched between two *nipi* diodes.

To validate the *ADEP* model, profiles were generated for each measurement condition employed in generating the results depicted in Fig. 3. The active region of the device was chosen as the top 1.2 μm since the heavily doped AlInP back surface field layer should act as a barrier to holes generated in the GaAs substrate. The integrated *ADEP* in the active region was calculated using (1) and (4) to arrive at the total rate of energy deposition within the active region of the diode. These values where all normalized to the magnitude of the measured I_{sc} for the 3.0 mm configuration. Fig. 4 contains the results of the normalized integrated *ADEP* calculations overlaid with the measured I_{sc} values (from the curves in Fig. 3) as a function of source–device separation. Very good agreement is observed between the normalized integrated *ADEP* and the measured I_{sc} values. This means that the geometry of the device, the energy deposited in air, and the energy deposited in the InGaP diode were all accurately modeled since all three are functions of the source–device separation.

At zero bias, the short circuit current is approximately equal to the alpha generated current and therefore, the normalization parameter is equal to η_α as indicated from (4). For a short circuited solar cell under a monochromatic light bias the illumination current can subsequently be broken down as the excitation power times the spectral response of the device for that wavelength: $I_{sc}(\lambda) = \eta_{SR}(\lambda) P_{\text{in}}(\lambda)$. The spectral response is typically defined in terms of A/W, which is analogous to the number of extracted electrons per eV of energy, reaching a maximum value of 1/*hv* where *hv* is the energy (in eV) of the exciting monochromatic light. Similarly, the value used to normalize the incident *ADEP* power to the short circuit current η_α can be described as the "alpha-response" and the value measured here was 0.3 electrons per eV.

The spatial variations in the *ADEP* and the D^3P within the InGaP diode under the ^{210}Po alpha-particle source and experimental configuration used to measure the flux dependant I–V response are provided in the left and right sections of Fig. 5, respectively. Here the source–device separation was modeled as 2.0 mm, which is the distance used to monitor the power output and radiation tolerance of similar InGaP devices [3]. The intensities of the contour plots were normalized to allow for comparison since the *ADEP* maximum intensity is approximately five

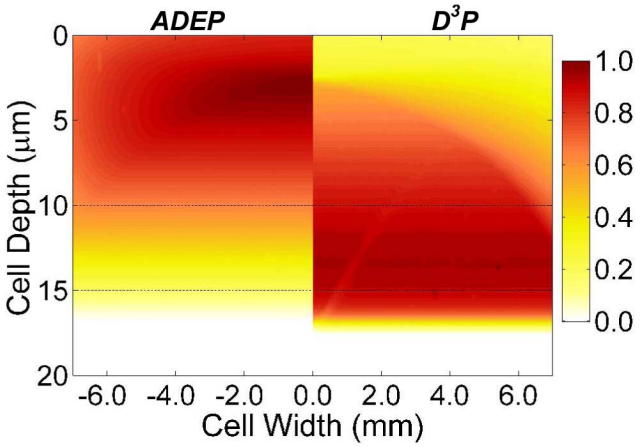

Fig. 5. Contour plots depicting the spatial variation of the normalized *ADEP* (left) and normalized D^3P (right) for an InGaP device under a ^{210}Po isotropic alpha-particle source.

orders of magnitude greater than that of the D^3 P maximum intensity. In this configuration, there is a favorable spatial separation between the regions of maximum *ADEP* and those of maximum D^3P suggesting an optimal thickness that maximizes the objective of long term power output (i.e., alpha-particle-generated current with minimal lattice defect generation). When modeled with a minimum separation (not shown), the *ADEP* and D^3P both peak at the surface and drop off monotonically with increasing depth into the device (a small separation, 20 μm, was required due to the numerical procedure employed in the calculations) [3]. This configuration, which is consistent with the expected final radioisotope battery design, does not have the favorable separation between regions of high energy and high damage deposition. However, this information may be useful in futures studies to alter the device structure so that the *ADEP* or the D^3P are balanced throughout each junction within the device.

TABLE I
EXTRACTED VALUES FOR THE CURVE FITTING PARAMETERS FROM (3) AND (5) BASED ON DARK AND ILLUMINATED I–V RESPONSE FOR THE p^+n INGAP DIODE

Symbol	Value	Units
I_{o1}	35.8	fA/cm^2
I_{o2}	2.86	pA/cm^2
n_1	1.53	N.A.
n_2	2.11	N.A.
R_{SHO}	2	GΩ
k	87.5×10^6	cm^2/A

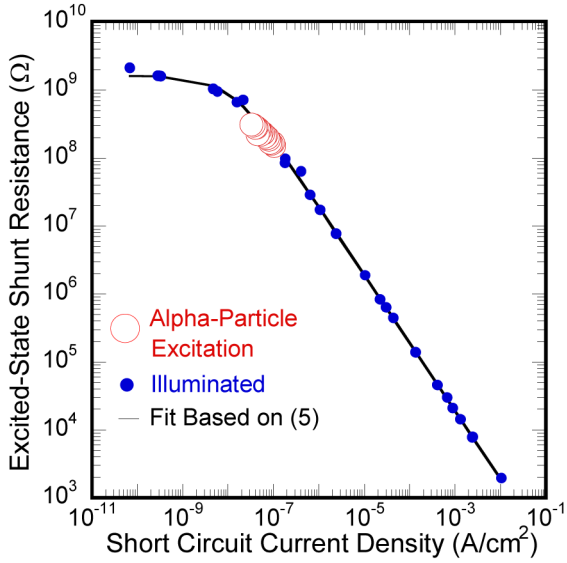

Fig. 6. The measured excited-state shunt resistance versus short circuit current density for an InGaP device under photon illumination (blue circles) and under alpha-particle irradiation (red circles). The solid line in the figure is the minimized least squares curve fit of (5) to the illuminated excited-state R_{SH} versus I_{sc} data.

B. Simulated Nipi Device Performance

The parameters used to simulate the *nipi* device performance were based on the p^+ n InGaP diodes as discussed in Section II. The dark diode curve fitting parameters from the p^+ n device are provided in Table I. The magnitude of the I_{o2} parameter exceeds that of the I_{o1} indicating that recombination current dominates the device operation under low forward bias (i.e., $<$ 0.8 V). The ideality coefficients and a V_{oc} of 1.25 V under AM0 illumination indicate a nearly ideal operation approaching that obtained by state-of-the-art InGaP diodes [16]. Consequently, the *nipi* device performance simulated based on the parameters of this single junction diode represents the performance of a realistic device with the theoretical limiting performance being only slightly higher. Furthermore, theoretical or experimental diode parameters of other optimized single junction p^+n or *pin* devices can easily be substituted into the model without loss of validity.

In addition to the dark diode parameters, the free parameters in (5) relating to the excited-state $R_{\rm SH}$, have been determined by calculating the inverse-reverse-bias slope (between -0.3 V—0 V) as a function of illumination intensity. Fig. 6 contains a plot of the measured excited-state $R_{\rm SH}$ plotted with respect to the measured I_{sc} of the device under photo- and alpha-particle excitation. Since the I_{sc} is linearly related to the incident excitation power, this plot is comparable to a plot of excited-state R_{SH} versus excitation power. For I_{sc} levels greater than 0.1 μA/cm ^{2} the excited-state R_{SH} is inversely proportional to I_{sc} (i.e., excitation power) and is consistent with a linear increase in junction conductance with excitation power. Below 0.1 μA/cm ^{2} the photo- (alpha-particle) generation rate within the space charge region of the device becomes comparable to un-excited conditions and asymptotically reaches the dark current value at $I_{sc} \sim 10^{-9}$ A/cm^2. The solid line in Fig. 6 is a fit of (5) to the illuminated excited-state R_{SH} data (blue circles) and is in good agreement with the measured results (the values obtained for the curve fitting parameters used in (5) are provided in Table I). Interestingly, the alpha-particle excited-state R_{SH} values (red circles) follow the same trend suggesting that the excited-state R_{SH} dependence on bias is a space-charge-region dominated effect since the spatial excitation profiles within the device will be drastically different under illumination and alpha-particle excitation sources.

The *nipi* device performance has been simulated using (3) wherein the parameters from Table I were employed in addition to a specific I_α value for each *pin* or *nip* device in the multi-junction stack. In a *nipi* device, each doped layer (with the exception of the top and bottom most layers) will form a junction with the oppositely doped layer above and below it. Therefore in the simulated structure, the top layer is modeled as a 0.5 μm n-type layer, followed by a 0.2 μm intrinsic region, and a 1.0 μm p-type layer. The thickness of the remaining layers is 0.2 μm for the intrinsic regions and 1.0 μm for the doped regions except for the bottom most layer which is 0.5 μm. This leads to stacked *pin/nip* junctions each of which are 1.2 μm thick and comparable to the p^+n device from which the dark diode fitting parameters were obtained. Two excitation configurations were simulated, one consisted of a source–device separation of 20 μm, while the other was simulated with a separation of 2000 μm, both having a source flux of 20 mCi/cm^2. The I_α was calculated for each single junction device based on its position within the multi-junction stack using (4) and an *ADEP* calculated for both values of source–device separation.

Fig. 7 contains the simulated power output, V_{oc}, and the internal and external efficiencies as a function of the number of 1.2 μm junctions in the multilayered *nipi* stack. In both configurations, the V_{oc} of the simulated *nipi* device follows a trend which is similar to the *ADEP* profile along a path normally incident into the device. From Fig. 5, the location of maximum alpha-particle energy deposition occurs $\sim 5\mu$m into the device. This corresponds to a five junction *nipi* device configured with a 2000 μm source–device separation. The maximum voltage is observed in a 1-junction device when simulated with a minimum separation since the peak alpha-particle energy deposition occurs at the surface. The parallel connectivity of the devices causes the current to continually increase with increasing number of junctions, following a trend similar to the integrated energy deposited along a path normally incident into the device. The decreasing voltage and increasing current yield a maximum in the power output curve at 14 junctions for both simulated *ADEP* profiles (i.e., source–device separations). This corresponds to a total active region thickness of about 16.8 μm, which approaches the limit of high quality epitaxially grown InGaP. However, based on the modeling results, it is apparent that devices containing 8–10 junctions (i.e., 9.6–12.0 μm of active thickness) will achieve nearly the same power output. This could reduce the thickness of the active region by nearly a factor of two making the growth of such a structure more feasible.

The internal efficiencies for each configuration are directly proportional to the power output curves and nearly equal for both of the simulated source–device separations, regardless of the number of junctions simulated in the device. If the power output from the device is defined as: $P_{mp} \equiv ffV_{oc}I_{sc}$, where *ff* is the fill factor, then from (4) and (12) it can be shown that $\eta_i = ffV_{oc}\eta_\alpha$. Therefore, the internal efficiency will be similar for two different source–device separations provided the level of flux is sufficient to generate a comparable V_{oc} in both configurations. The external efficiencies of the device under the two geometric configurations follow a similar trend as the internal efficiency but are lower for the 2000 μm configuration since additional energy is dissipated by the alpha-particles traversing

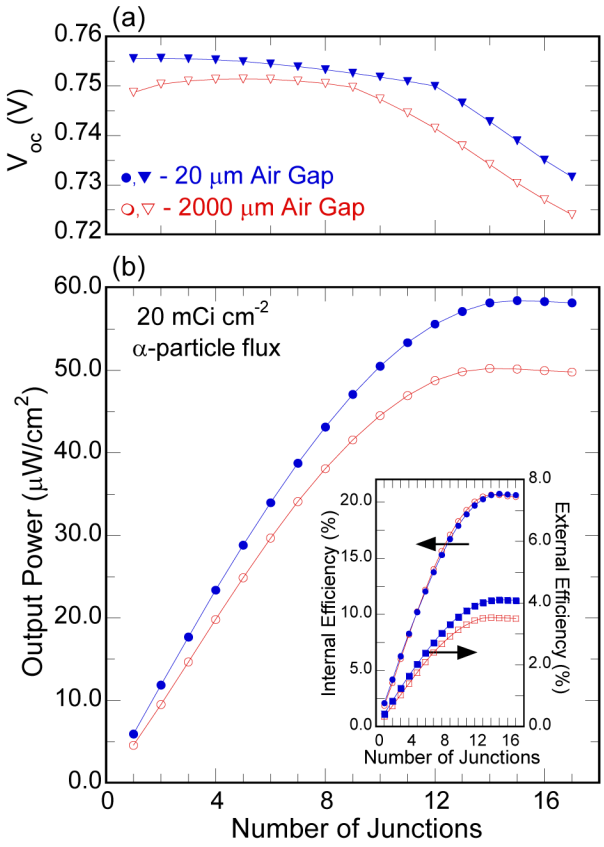

Fig. 7. The (a) open circuit voltage and (b) output power as a function of the number of junction within a simulated *nipi* device under 20 mCi/cm ^{2} alpha-particle flux for two different source–device separations: 20 μm (blue/filled circles and triangles), and 2000 μm (red/open circles and triangles). The inset contains the internal and external efficiencies for the two separations. Lines are provided as visual aids guide to the eye.

the larger air gap. Like the power output, the difference in external efficiencies for the two devices is more pronounced as the number of junctions increases (i.e., the larger air gap reduces the maximum alpha-particle range). The maximum external efficiencies were 4.1%, and 3.6% for the 20 μm, and 2000 μm configurations, respectively.

The efficiencies and power output illustrated in Fig. 7 pertain to the specific level of flux used (20 mCi/cm^2) and would be sufficient to meet the power requirements of a low power wireless microsystem device [1]. However, under larger fluxes the I_{sc}, V_{oc}, and *ff* will increase leading to a super-linear dependence of the power output and efficiency (internal and external) on flux. This super-linear dependence is illustrated in Fig. 8 wherein the simulated open circuit voltage and output power for *nipi* devices with total active thicknesses of 16.8 μm and comprised of *nip/pin* single junction devices (0.4–2.0 μm sub-device junction thickness) are plotted with respect to the source activity on a semi-log scale. The linear trend in the open circuit voltage in the figure indicates that the expected logarithmic dependence on source activity is realized. The product of the voltage and the linearly increasing current with source activity (based on (3) and (4)) yields a super-linear dependence in power output as shown in Fig. 8. It is important to note that increases in activity will have the adverse effect of shorter lifetimes. However, nearly

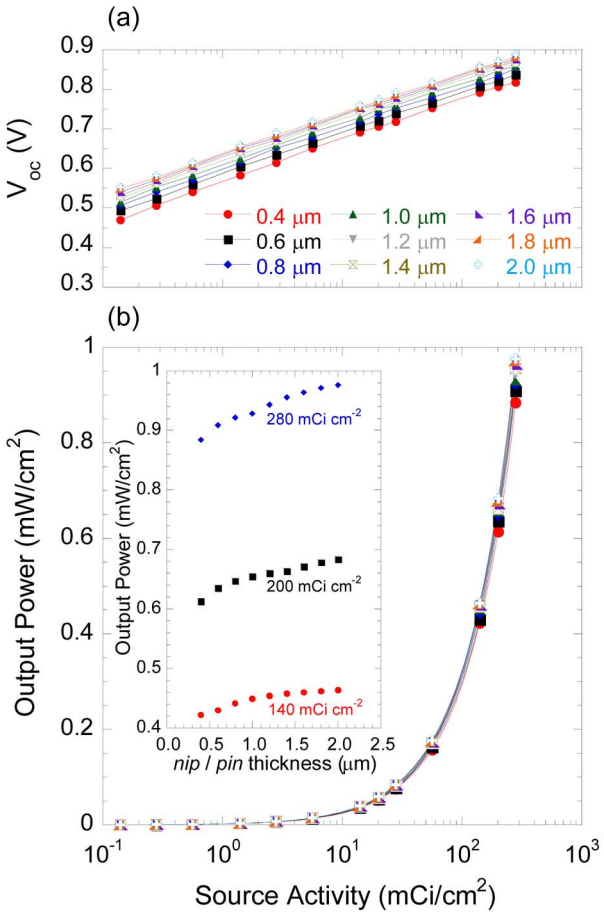

Fig. 8. Semi-log plots of the simulated open circuit voltage (a) and power output (b) of a as a function of source activity for *nipi* devices with an active thickness of 16.8 μm and various single device *nip/pin* thicknesses. The inset contains the power output as a function of single device thickness for three different source activities. Lines are provided as visual aids to the guide the eye.

1 mW can be obtained from a 1 cm^2 device which is coupled to a 280 mCi source operating with an efficiency of over 10.4%. This can be doubled if a sandwich structure were employed and would further increase if the area of the source were matched to that of the device.

The inset in Fig. 8 demonstrates the effect of different sub-device junction thicknesses on the power output of the total *nipi* device stack. A small improvement is obtained by increasing the thickness of the sub-devices (i.e., thicker layers with fewer junctions), but increases in sub-device thickness may result in adverse radiation tolerance effects due to the increased length required for minority carriers to reach the space-charge-region. However, the thicker layers may allow for improved rectification at the selectively doped regions since the contacting scheme relies on selective contacting. It is important to note that the lumped parameter equivalent circuit model does not take into account the electronic properties (e.g., recombination lifetimes, two-dimensional sub-band structure, carrier concentration) that become tunable parameters in *nipi* structures when the doping period is reduced to a few hundred nanometers or less [17]. Additionally, the dependence of radiation tolerance on sub-device thickness has not yet been investigated. The flexibility of the lumped parameter equivalent circuit model will allow for such effects to be investigated in the future simply by incorporating the trends observed in measurements on single junction devices.

The *nipi*-diode structure investigated here is expected to have an increased radiation tolerance over that of abrupt junction devices since a vertical drift field is employed in the extraction of carriers. A slight lateral drift field will also be present at the heavily doped region assisting in the collection of the separated electrons and holes. Furthermore, once the electrons or holes are separated to their respective n-type and p-type layers (by the vertical drift field) they become majority carriers; the lifetimes of majority carriers are much larger than that of minority carriers under low injection conditions. In this configuration, the active region of the device is isolated from the defects which are generated within the substrate. This is in contrast to traditional vertical conduction solar cells which require conduction through the substrate. As noted above, the D^3P profile can be used to investigate the spatial extent of the displacement damage, enabling one to design a layered structure and device geometry in which the damage occurring in the active region of the device is minimized. Even with these improvements, degradation due to alpha-particle induced lattice defects remains the determining factor in the operating lifetime of the device.

To relate the D^3P to the device lifetime, the characteristic degradation equation which describes the variation of diodes when the degradation is dominated by a reduction in the of the minority carrier diffusion lengths [16], can be employed:

$$\boldsymbol{P}_{\max}(\boldsymbol{t}) = \boldsymbol{P}_{\max,0} - \boldsymbol{C}\log\left(1 + \frac{\boldsymbol{t\varphi NIEL}_{\text{eff}}}{\boldsymbol{D_x}}\right) \tag{12}$$

with

$$\boldsymbol{NIEL}_{\text{eff}} \equiv \int_{\boldsymbol{v}} \boldsymbol{D}^3\boldsymbol{P}(\boldsymbol{\Phi}=1,\boldsymbol{v})\,\boldsymbol{dv}. \tag{13}$$

In (12), the effective non-ionizing energy loss $(\text{NIEL}_{\text{eff}})$ for the specific device geometry and energy of alpha-particle was employed. (A similar methodology would also apply for beta-particle sources.) This was determined, in (13), by integrating the D^3P over the entire active-region volume v and setting the total fluence equal to one $\Phi = 1$. Using these equations, one may estimate the power output of a *nipi*-diode as a function of time t by inserting the empirical values of C and D_x which are specific for each material system. The use of the *nipi*-structure may be effective at increasing the value of D_x since it depends on the material and the structure of the device [16]. However, from (12) it is also evident that spreading the source flux φ between multiple *nipi*-diodes would reduce the rate of degradation at the price of a slightly reduced η_e.

V. Conclusion

A framework for modeling *nipi* devices under an isotropic alpha-particle source has been presented. The *ADEP* profile was verified experimentally by comparing the short circuit current of an InGaP diode as a function of source–device separation, to the calculated total energy deposited within the device based on the *ADEP*s modeled for each experimental configuration. A strong correlation between the measured and calculated values was observed which allowed for an alpha-response value of 0.3 electrons per eV to be determined.

The *ADEP* profile was used to obtain the generation current for the lumped parameter equivalent circuit model allowing *nipi* devices to be simulated as a multiple junction device, consisting of single junction *pin* and *nip* devices connected in parallel. To allow many orders of magnitude in power output to be simulated, an empirical function describing the effects of excitation power on the excited-state shunt resistance was included. The performance of multi-junction *nipi* stacks consisting of varying numbers of single junction devices and single junction device thicknesses were simulated as a function of fluence.

The results of these simulations indicate that the number of sub-device junctions of a *nipi* device necessary to achieve the maximum voltage corresponds to the number of sub-devices needed to reach the location of the *ADEP* peak maxima. In contrast, the current density output follows the integrated *ADEP* profile and therefore continues to increase with each additional junction until the maximum range of the alpha-particles is encountered. For peak power output a device containing an active region thickness of ~ 16.8 μm would be required, though $> 75\%$ of the peak power could be achieved with little over half of that thickness. A power output of 2 mW/cm^2 was predicted for a bi-layered device coupled with a 300 mCi/cm^2 alpha-particle source, excluding radiation damage effects. Increased lifetime may be achieved if the source is spread between multiple bi-layered devices; albeit at the cost of a slightly reduced nuclear-to-electrical conversion.

REFERENCES

[1] S. Roundy, P. K. Wright, and J. Rabaey, *Comput. Commun.*, vol. 26, pp. 1131–1144, 2003.

[2] K. E. Bower, Y. A. Barbanel, Y. G. Shreter, and G. W. Bohnert, *Polymers, Phosphors, and Voltaics for Radioisotope Microbatteries*. Boca Raton, FL: CRC Press, 2002, vol. 1, p. 477.

[3] C. D. Cress, B. J. Landi, D. M. Wilt, and R. P. Raffaelle, *J. Appl. Phys.*, vol. 100, 2006, 114519(1–5).

[4] M. V. S. Chandrashekhar, C. I. Thomas, H. Li, M. G. Spencer, and A. Lal, *Appl. Phys. Lett.*, vol. 88, 2006, 033506(1–3).

[5] R. J. Walters, S. R. Messenger, G. P. Summers, M. J. Romero, M. M. Al-Jassim, D. Araujo, and R. Garcia, *J. Appl. Phys.*, vol. 90, pp. 3558–3565, 2001.

[6] G. Rybicki, C. Vargas-Aburto, and R. Uribe, in *Proc. 25th IEEE Photovoltaic Specialists Conf. (PVSC)*, 1996, pp. 93–96.

[7] A. L. Barry, B. Lehmann, D. Fritsch, and D. Braunig, *IEEE Trans. Nucl. Sci.*, vol. 38, no. 6, pp. 1111–1115, Dec. 1991.

[8] A. Ionascut-Nedelcescu, C. Carlone, A. Houdayer, H. J. v. Bardeleben, J.-L. Cantin, and S. Raymond, *IEEE Trans. Nucl. Sci.*, vol. 49, no. 6, pp. 2733–2738, Dec. 2002.

[9] W. Sun, N. P. Kherani, K. D. Hirschman, L. L. Gadeken, and P. M. Fauchet, *Adv. Mater.*, vol. 2005, pp. 1230–1233, 2005.

[10] S. G. Bailey, D. M. Wilt, S. L. Castro, C. D. Cress, and R. P. Raffaelle, "Photovoltaic development for alpha voltaic batteries," in *Proc. 31st IEEE Photovoltaics Specialist Conf.*, 2005, pp. 106–109.

[11] K. W. Goossen, J. E. Cunningham, and W. Y. Jan, *Appl. Phys. Lett.*, vol. 57, p. 744, 1990.

[12] K. W. Goossen, J. E. Cunningham, W. Y. Jan, and D. A. B. Miller, *IEEE Photon. Technol. Lett.*, vol. 5, no. 2, pp. 181–183, Feb. 1993.

[13] S. R. Messenger, E. A. Burke, G. P. Summers, and M. A. Xapsos, *IEEE Trans. Nucl. Sci.*, vol. 46, no. 6, pp. 1595–1602, Dec. 1999.

[14] J. F. Ziegler, J. P. Biersack, and U. Littmark, *The Stopping and Range of Ions in Solids*. New York: Pergamon, 1985, vol. 1.

[15] S. M. Sze, *Physics of Semiconductor Devices*, 2nd ed. New York: Wiley, 1981.

[16] R. J. Walters, M. A. Xapsos, H. L. Cotal, S. R. Messenger, G. P. Summers, P. R. Sharps, and M. L. Timmons, *Solid-State Electron.*, vol. 42, pp. 1747–1756, 1998.

[17] G. H. Dohler, *IEEE J. Quantum Electron.*, vol. QE-22, no. 9, pp. 1682–1695, Sep. 1986.